17

Monitoring Soil Moisture from Spaceborne Passive Microwave Radiometers: Algorithm Developments and Applications to AMSR-E and SSM/I

Hui Lu[1*], Toshio Koike[1], Tetsu Ohta[1], David Ndegwa Kuria[2], Kun Yang[3], Hideyuki Fujii[4], Hiroyuki Tsutsui[1] and Katsunori Tamagawa[1]
[1]*The University of Tokyo, Japan*
[2]*Jomo Kenyatta University of Agriculture and Technology, Kenya*
[3]*Institute of Tibetan Plateau Research, Chinese Academy of Sciences, China*
[4]*Japan Aerospace Exploration Agency, Japan*

1. Introduction

Soil moisture patterns, both spatial and temporal, are the key to understanding the spatial variability and scale problems that are paramount in scientific hydrology, meteorology and climatology. Soil moisture controls the ratio of runoff and infiltration (Delworth & Manabe, 1988; Wagner et al., 2003), decides the energy fluxes (Entekabi et al., 1996; Prigent et al., 2005) and influents vegetation development and then carbon cycle. A long term soil moisture data set on a region scale therefore could provide valuable information for researches such as climate change and global warming (Seneviratne et al., 2006), and then improve the weather forecasting (Beljaars et al., 1996; Schar et al. , 1999) and water resources management.

Soil moisture profile can be observed at point scale by using gravimetric sampling or some automatic probes, such as Time Domain Reflectometry (TDR), Neutron Probe (NP), etc. These methods are commonly used to provide accurate and continuous soil moisture information and adopted by the meteorology, hydrology and agriculture stations. But these point information are not enough for the regional research and application, and are also not available in the remote areas where difficult to access and to maintain such stations. On the other hand, satellite remote sensing offers a possibility to measure surface soil moisture at regional, continental and even global scales.

Although surface soil moisture can be estimated indirectly from visible/infrared remote sensing data (Verstraeten et al., 2006), it failed to produce routinely soil moisture map mainly due to factors inherent in optical remote sensing, such as atmosphere effects, cloud masking effects and vegetation cover masking effects. Fortunately, microwave remote sensing offers a possibility to observe area-averaged surface soil moisture regularly in the global scale, by directly measuring to the soil dielectric properties which are strongly related

*Corrosponding author and address: Dr. Hui LU, River and Envi. Eng. Lab., Dept. of Civil Eng., Univ. of Tokyo, Hongo 7-3-1, Bunkyo-ku, Tokyo, 113-8656, Japan. Tel. 81-3-5841-6109 Fax: 81-3-5841-6130 E-mail: lu@hydra.t.u-tokyo.ac.jp

to the liquid moisture content (Hipp, 1974). Moreover, extra advantages of microwave remote sensing include: (1) long wavelength in microwave region which enable the low frequency microwave signals to penetrate clouds and to provide physical information of the land surface; and (2) independent of illumination source which enables the spaceborne sensors to observe earth all-day with all-weather coverage.

There are two approaches through which microwave remote sensing estimating surface soil moisture: active ways by Radar and/or Synthetic Aperture Radar (SAR) with high spatial resolution (in the order of ten to hundred meters) and long revisiting period (about 1 month), passive ways by radiometers with coarse resolution (~ order of 10 km) and frequent temporal coverage (daily or bi-daily). Considering the temporal resolution requirement of the meteorological and hydrological modeling, passive ways are more suitable for the application in these fields and have been wildly used in recent 30 years.

Although it was recognized early that microwave sensors operated at L-band (1-2GHz) provide the best surface soil moisture observation (Schmugge et al. 1988), L-band radiometers are not equipped on any satellites. This situation is mainly due to the limitation of our current technical capability, which is a significant challenge to built L-band antenna big enough to provide reasonable resolution. So all current available passive microwave remote sensing data are observed by radiometers operating with higher frequencies, such as the Scanning Multichannel Microwave radiometer (SMMR; 6.6, 10.7, 18.0, 21 and 37 GHz) on board Nimbus-7 Pathfinder (Gloersen & Barath, 1977), the Special Sensor Microwave Imager (SSM/I; 19.35, 22.2, 37.0 and 85.5 GHz) on board Defense Meteorological Satellite Program (DMSP) (Hollinger et al., 1990), and the Advanced Microwave Scanning Radiometer (AMSR-E; 6.925, 10.65, 18.7, 23.8, 36.5 and 89 GHz) of the Earth Observing System (EOS) on board Aqua (Kawanishi et al., 2003). Among them, AMSR-E is the only passive systems which including surface soil moisture as a target product. In terms of continuous observation, SSM/I series, starting from 1987, is highly expected to provide long-term global soil moisture estimation.

A number of techniques have been used to estimate surface soil moisture information from microwave remote sensed data, such as statistical inversion (Njoku & Kong, 1977), artificial neural networks (Said et al., 2008), and genetic algorithm (Singh & Kathpalia, 2007). However, only the radiative transfer-based methods are considered as the true retrieval, for both passive and active techniques. The radiative transfer models adopted in those methods generally are consists of three parts: a dielectric model (Wang & Schmugge, 1980; Dobson et al., 1985; Mironov et al., 2004) which relating surface soil moisture content to the dielectric constants; a surface roughness model (Choudhury et al., 1979; Fung et al., 1992; Wegmuller & Matzler, 1999; Chen, et al. 2003; Shi, et al. 2005) which accounting for surface scattering effects; and a vegetation layer model (Ulaby et al., 1983; Paloscia & Pampaloni, 1988; Jackson & Schmugge, 1991) which accounting for the vegetation masking effects.

Algorithms considering various other factors have also been proposed to retrieve soil moisture content from passive microwave remote sensed data. T. Jackson (Jackson, 1993) developed a so-called single channel algorithm (SCA), in which the brightness temperature of the 6.9 GHz horizontal polarization channel was used. In this algorithm, ancillary data such as air temperature, land cover, Normalized Difference Vegetation Index (NDVI), surface roughness, and soil texture and porosity are needed. The algorithm of Njoku et al (Njoku & Entekhabi, 1996; Njoku et al., 2003) is a multiple channel iterative retrieval algorithm. It uses the brightness temperature observed by the lowest six channels of AMSR-

E. Using their algorithm, the surface temperature, the vegetation opacity and the soil moisture are estimated simultaneously. The algorithm proposed by Paloscia (Paloscia et al., 2001; 2006) is an experiment-based linear regression retrieval, in which soil moisture is estimated by using both the Polarization Index (PI) at 10.7GHz and the brightness temperature at 6.9GHz.

After more than 20 years effort, good results were obtained and several global and continental scale soil moisture datasets (e.g. Njoku et al. 2003; Owe et al. 2008) were generated. But both the quality and application region of these algorithms can be further improved. For example, Shibata et al. (2003) pointed out that the soil moisture in desert regions retrieved from AMSR-E soil moisture algorithms indicate very wet areas. To solve such problem, the forward model, viz. Radiative Transfer Model (RTM) should be improved firstly.

In this study, we present a new soil moisture retrieval algorithm developed at the University of Tokyo. This algorithm is based on a modified radiative transfer model (Lu et al., 2006), in which the volume scattering inside soil layers is calculated through dense media radiative transfer theory (DMRT) (Wen et al., 1990; Tsang & Kong, 2001) and the surface roughness effect is simulated by Advanced Integration Equation Model (AIEM) (Chen et al., 2003). The optimal values of forward model parameters are estimated using in situ observation data and lower frequency brightness temperature data. And with those optimized parameters, we run the forward model to generate a lookup table, which relates the variables of interest, such as soil moisture content, soil physical temperature, vegetation water content and atmosphere optical thickness, to the brightness temperature or some indexes calculated from brightness temperature data. Finally, soil moisture content is estimated by linearly interpolating the brightness temperature or index into the inversed lookup table. The algorithm was validated by using the AMSR-E match up data set at Mongolia region. Moreover, the capability of our algorithm to retrieve soil moisture from SSM/I was also checked at the same region.

The paper is organized as follows. In Section 2, we present our physically-based radiative transfer model, emphasizing the soil RTM, so-called DMRT-AIEM model. In Section 3 we describe the structure of our algorithm. Section 4 and 5 discusses the application of our new algorithm on AMSR-E and SSM/I data, respectively. Section 6 contains some concluding remarks.

2. The Forward Model: A Fully Physically-based Radiative Transfer Model

Our algorithm is based on a look up table, which is a database of brightness temperature simulated by a radiative transfer model for various possible conditions. The quality of retrieved soil moisture, therefore, is heavily dependent on the performance of the radiative transfer model. So, the main task of our algorithm development was to develop a physically-based soil moisture retrieval algorithm, which is able to estimate soil moisture content from low frequency passive microwave remote sensing data and to overcome the misrepresent problems occurred in dry areas.

2.1 The radiative transfer process for land surface remote sensing

For the land surface remote sensing by spaceborne microwave radiometers, the radiative transfer process from land to space can be divided into as four stages as follows:

(1) Radiative transfer inside soil media.
The initial incident energy is treated as the one starting from the deep soil layer, which propagates through many soil layers, attenuating by the soil absorption effects (dominative at wet cases) and volume scattering effects (dominative at dry cases), experiencing multi-reflection effects between the interfaces of soil layers, finally reaching the soil/air interface.
(2) Surface scattering process at soil/air interface.
At the soil/air interface, the surface scattering influences this upward initial radiation by changing its direction, magnitude and polarization status. At the same time, the downward radiation from the cosmic background, atmosphere, precipitation and canopy are reflected by the air/soil interface, and parts of the reflected radiation propagate along the same direction as that emitted from the soil layers.
The upward radiation just above the soil/air interface, therefore, is not only the product of soil medium but also the product of downward radiation.
(3) Radiative transfer inside vegetation layers.
After leaving the soil/air interface, the upward radiation propagates through the canopy layer (if there are vegetations), experiences the volume scattering effects from the leaves and stems of vegetations and the multi-reflection effects between canopy/air and soil/air interfaces. At the same time, parts of the upward radiation from vegetations join our target radiation.
(4) Radiative transfer inside atmosphere layers.
After transmitting from vegetation layer, the radiation continues its way, traversing the cloud and precipitation layers, affected by the absorptive atmosphere gases, scattered by precipitation drops, incorporating the emission from surroundings, finally detected by the sensors boarded on satellites.
The story of radiative transfer is so complicate that make it necessary to simplify the process to make it computable. In microwave region, the reflectivity of the air/soil interface is generally small. The downward radiation from vegetation and rainfall, which is reflected by the soil surface, therefore, is neglected. Moreover, for the lower frequencies region of microwave, the atmosphere is transparent. Finally, after neglecting all the downward radiation and parts of upward radiation from surroundings, the radiative transfer model is written as:

$$T_b = T_{bs}e^{-\tau_c}e^{-\tau_r} + (1-\omega_c)(1-e^{-\tau_c})T_c e^{-\tau_r} + \int(1-\omega_r(R))(1-e^{-\tau_r(R)})T_r(R)dR \quad (1)$$

where T_{bs} is the emission of the soil layer, T_c is the vegetation temperature, T_r is the temperature of precipitation droplets, τ_c and ω_c are the vegetation opacity and single scattering albedo, and τ_r and ω_r are the opacity and single scattering albedo of precipitation.
For the frequencies less than 18GHz, equation (1) can be even simplified by omitting the precipitation layer, as:

$$T_b = T_{bs}e^{-\tau_c} + (1-\omega_c)(1-e^{-\tau_c})T_c \quad (2)$$

2.2 Radiative process inside soil media: profile effects and volume scatting effects

Microwave can penetrate into soil media, especially for dry cases, in which the penetration depth of C-band is about several centimeters. The soil moisture observed by microwave remote sensing, therefore, is inside a soil media with a volume of several centimeters depth.

The radiative transfer process inside a soil media includes various effects, such as moisture and temperature profile effects and the volume scattering effects of dry soil particles. To simulate these effects, the dielectric constant model should be addressed at first.

(1) Dielectric constant model of soil

In the view of microwave, soil is a multi-phase mixture, with a dielectric constant decided by moisture content, bulk density, soil textural composition, soil temperature and salinity. In our algorithm, the dielectric constant of soil is calculated using Dobson model (Dobson et al., 1985):

$$\varepsilon_{soil}^{\alpha} = 1 + \frac{\rho_b}{\rho_{ss}}(\varepsilon_{ss}^{\alpha} - 1) + m_v^{\beta}\varepsilon_{fw}^{\alpha} - m_v \tag{3}$$

where ρ_b is the bulk density of soil, ρ_{ss} = *2.65* is the density of solid soil particle; ε_{ss} = *(4.7, 0.0)* is the dielectric constant of soil particle; m_v is the volumetric water content; ε_{fw} is the dielectric constant of free water, can be calculated by the model proposed by Ray (Ray, 1972); a=*0.65* is an empirical parameter; and β is a soil texture dependent parameter as follows:

$$\beta = 1.09 - 0.11S + 0.18C \tag{4}$$

where *S* and *C* are the sand and clay fraction of the soil, respectively.

(2) Profile effects of soil media

The heterogeneity inside soil media causes the so-called profile effects. The profile effects can be accounted for by using the simple zero-order noncoherent model proposed by Schmugge and Choudhury (1981) or by more complicate first-order noncoherent model given by Burke et al. (1979). The volume scattering effects inside soil media are not included in both models.

In order to include the volume scattering effects, a more complicate model was adopted in our algorithm. We assumed that the soil has a multi-layer structure and is composed of many plane-parallel and azimuthally symmetric soil slabs with spherical scattering particles. The radiative transfer process in a plane-parallel and azimuthally symmetric soil slab with spherical scattering particles can be expressed as (Tsang & Kong, 1977) :

$$\mu\frac{d}{d\tau}\begin{bmatrix} I_v(\tau,\mu) \\ I_h(\tau,\mu) \end{bmatrix} = \begin{bmatrix} I_v(\tau,\mu) \\ I_h(\tau,\mu) \end{bmatrix} - (1-\omega_0)B(\tau)\begin{bmatrix} 1 \\ 1 \end{bmatrix} - \frac{\omega_0}{2}\int_{-1}^{1}\begin{bmatrix} P_{VV} & P_{VH} \\ P_{HV} & P_{HH} \end{bmatrix}\begin{bmatrix} I_v(\tau,\mu') \\ I_h(\tau,\mu') \end{bmatrix} d\mu' \tag{5}$$

where $I_P(\tau,\mu)$ is the radiance at optical depth τ ($d\tau$=$K_e dz$, with extinction coefficient K_e and layer depth dz) in direction μ for polarization status P (horizontal or vertical), ω_0 is the single scattering albedo of a soil particle, $B(\tau)$ is the Planck function and P_{ij} (i,j=*H or V*) is the scattering phase function. The 4-stream fast model proposed by Liu (Liu, 1998) solves (5) by using the discrete ordinate method and assuming that no cross-polarization exist. The Henyey-Greenstein formula (Henyey & Greenstein, 1941) is used to express the scattering phase function.

(3) Volume scattering effects of dry soil particles

With considering the facts that the soil particles are densely compacted, the multi-scattering effects of soil particles should be accounted for. In our algorithm, this volume scattering

effect were calculated by the so-called dense media radiative transfer theory (DMRT) under Quasi Crystalline Approximation with Coherent Potential (QCA-CP) (Wen et al., 1990; Tsang & Kong, 2001). Dense Media radiative transfer theory was derived from Dyson's equation under the quasi-crystalline approximation with coherent potential (QCA-CP) and the Bethe-Salpeter equation under the ladder approximation of correlated scatterers.

By using the DMRT, the extinction coefficient K_e and albedo ω used in equation (5) were calculated. And then the radiance of each soil slab was calculated by the 4-stream fast model. The radiance just below the soil/air interface was obtained by integrating the radiance from bottom layer to the top layer. Finally, the apparent emission of soil media, T_{bs} in equation (1) and (2), was obtained.

2.3 Surface roughness effects

When an electromagnetic wave reaches the air/soil interface, it suffers the reflection and refraction due to the dielectric constant changing in the two sides of the interface. The roughness of the interface divides the reflected wave into two parts, one is reflected in the specular direction and another is scattered in all directions. Generally, the specular component is often referred to as the coherent scattering component. And the scattered component is known as the diffuse or noncoherent component, which consists of power scattered in all directions but with a smaller magnitude than that of the coherent component. Qualitatively, surface roughness increases the apparent emissivity of natural surfaces, which is caused by increased scattering due to the increase in surface area of the emitting surfaces. And it was demonstrated by many researches that the surface roughness has a nonnegligible effects on the accuracy of soil moisture retrieval by spaceborne microwave sensors (Oh & Key, 1998; Singh et al., 2003). In general, the surface roughness effects are simulated by two ways: semi-empirical models and fully physical-based models.

(1) Semi-empirical models

The semi-empirical models are simply and do not cost too much computation efforts. The parameters used in semi-empirical models are often derived from field observations. Depending on the parameters involved, there are three different semi-empirical models: Q-H model (Choudhury et al., 1979; Wang & Choudhury, 1981), Hp model (Mo & Schmugge, 1987; Wegmuller & Matzler, 1999; Wigneron et al., 2001) and Qp model (Shi et al., 2005).

(2) Fully physical-based model

In our algorithm, we simulated the land surface roughness effect using the Advanced Integral Equation Model (AIEM) (Chen et al., 2003). AIEM is a physically-based model with only two parameters: standard deviation of the height variations s (or *rms* height) and surface correlation length l. AIEM is an extension of the integral Equation Model (IEM) (Fung et al., 1992). It has been demonstrated that IEM has a much wider application range for surface roughness conditions than other models such as the Small Perturbation Model (SPM), Physical Optics Model (POM) and Geometric Optics Model (GOM). AIEM improves the calculation accuracy of the scattering coefficient compared with IEM by retaining the absolute phase term in the Green's function.

By coupling AIEM with DMRT (DMRT-AIEM), this radiative transfer model for soil media is fully physically-based. As a result, the parameters of DMRT-AIEM, such as the *rms* height, correlation length and soil particle size, have clear physical meanings and their values can be obtained either from field measurement or theoretical calculation.

2.4 Vegetation masking effects

The existence of canopy layers complicates the electromagnetic radiation which is originally emitted solely by soil layers. The vegetation may absorb or scatter the radiation, but it will also emit its own radiation. The effects of a vegetation layer depend on the vegetation opacity τ_c and the single scattering albedo of vegetation ω_c (Schmugge & Jackson, 1992). The vegetation opacity in turn is strongly affected by the vegetation columnar water content W_c. The relationship can be expressed as (Jackson & Schmugge, 1991):

$$\tau_c = \frac{b'\lambda^{\chi} W_c}{\cos\theta} \tag{6}$$

where λ is the wavelength, θ the incident angle, W_c the vegetation water content. χ and b' are parameters determined by vegetation type.

The single scattering albedo, ω_c, describes the scattering of the emitted radiation by the vegetation. It is a function of plant geometry, and consequently varies according to plant species and associations. The value of it is small in the low frequency microwave region (Palosica & Pampaloni, 1988; Jackson & Oneill, 1990). In our algorithm, ω_c is calculated by

$$\omega_c = \omega_0 \cdot \sqrt{W_c} \tag{7}$$

The value of albedo parameter ω_0 is decided empirically in current researches.Experimental data for this parameter are limited, and values for selected crops have been found to vary from 0.04 to about 0.12.

By combing the T_{bs} solved by equation (5), the surface reflectivity calculated by AIEM, the vegetation opacity τ_c calculated by equation (6), and the vegetation single scattering albedo ω_c estimated by equation (7), a physical-based radiative transfer model was developed.

3. The Algorithm

The basis of our algorithm is a data base of brightness temperature and/or some indexes calculated from brightness temperature. By searching the data base (or look up table) with the satellite observation as the input, soil moisture and other related variables of interest can be estimated quickly. Such high searching speed is the main reason why we adopt the look up table method for soil moisture retrieval. The implementation of our algorithm consists of three steps: (1) fixing the parameters used in the forward model; (2) generating a look up table by running forward model; and (3) retrieving soil moisture by searching the look up table.

3.1 Parameterization

As in other physically-based algorithms, such as that developed by Njoku et al. (2003) and the SCA developed by Jackson (1993), the parameters used in our algorithm have clear physical meanings. This advantage derives from the strength of the forward radiative transfer model. Before running the forward RTM to generate look up table, the parameters should be confirmed at first. The parameters to be confirmed include *rms* height (*s*), correlation length (*l*), soil particle sizes (*r*) and vegetation parameters such as χ and b'. Currently, we can obtain these parameters through two methods: best-fitting method and a

parameter optimization method supported by a Land Data Assimilation System developed in the University of Tokyo (LDAS-UT).

(1) Best-fitting method

For the region where in-situ soil moisture and temperature observation are available and when such observation are also representative, we can use a best-fitting way to optimize parameters. In order to simplify the calculation, low frequencies simulation and observation were used. These parameters are optimized by minimizing the cost function:

$$J(s,l,r,b',\chi,\ldots)=\sum_{i=1}^{n}\sum_{f}\sum_{p=H,V} ABS[TB_{sim}(i,f,p)-TB_{obs}(i,f,p)] \tag{8}$$

where the subscript *sim* denotes the model simulated value and *obs* is the observed value. n is the number of samples used in the optimization. p denotes the polarization status: H for horizontal polarization and V for vertical. f is some frequency in the long wavelength region where the atmospheric effect may be ignored, such as 6.9, 10.7 and 18.7 GHz of AMSR-E, 1.4 GHz of SMOS and 19GHz of SSM/I.

(2) Parameter optimization by LDAS-UT

For most remote regions, in-situ representative observation is not available. A more general parameter optimization method is proposed by Yang et al. (2007). In this method, long term (around 2 months) meteorological field was used to drive a land surface model (Simple Biosphere model, SiB2) to generate time series of soil moisture and temperature data set. And then corresponding TB was simulated with our RTM. Since the land surface parameter set (soil texture, porosity, particle size, roughness, etc.) was also used in SiB2, simulated soil moisture and temperature and corresponding TB were varying as the parameter set changes. By minimizing the difference between simulated TB and that of satellite observation, the best parameter set can be obtained. The optimized parameters by LDAS-UT, therefore, are depended on models and also influenced by the quality of forcing data. The detail of this method can be found from Yang et al. (2009).

3.2 Look up table generation

After Step 1, the optimal parameter values are then stored in the forward RTM. We then run the forward model by inputting all possible values of variables used in Equation (1), such as soil moisture content, soil temperature, vegetation water content and atmosphere optical thickness. A family of brightness temperatures is then generated. Based on this brightness temperature database, we select brightness temperatures of special frequencies and polarization to compile a lookup table or to calculate some indices to compile a lookup table. For example, in order to partly remove the influences of physical temperature, the ratio of TB at different frequencies and polarizations can be used. For instant, we can compile a look up table by using the index of soil wetness (ISW) (Koike et al., 1996; Lu et al., 2009), and Polarization Index (PI) (Paloscia & Pampaloni, 1988).

3.3 Soil moisture estimation

The lookup table generated in Step 2 is reversed to give a relationship which maps the brightness temperature or indices obtained from satellite remote sensing data to the variables of interest (such as soil moisture, soil temperature and vegetation water content).

Finally, we estimate soil moisture content by linear interpolation of the brightness temperature or indices into the inverted lookup table.

4. Application to AMSR-E Data Set

We tested our algorithm by retrieving soil moisture and temperature from AMSR-E TB data at a Coordinate Enhanced Observing Period (CEOP) (Koike, 2004) reference site in the Mongolian Gobi. The results were validated by comparing with in situ measurements byAutomatic Stations for Soil Hydrology (ASSH) and Automatic Weather Stations (AWS).

4.1 CEOP Mongolia reference site and AMSR-E match-up data set

The application region of this research is the AMPEX (ADEOS II Mongolian Plateau EXperiment for Ground Truth) area. AMPEX has joined the CEOP as the Mongolia reference site. AMPEX is designed to validate the AMSR and AMSR-E soil moisture algorithm(s). In this area, meteorological and land hydrological factors are measured with very densely installed instruments. AMPEX is located in the Mongolian Plateau, 235 km south of Ulan Bator. The area stretches 160km in the longitudinal direction (106°E~108°30 'E) and 120 km in the latitudinal direction (45°30N~47°N) on the Mandalgobi, where 6 AW Ss and 12 ASSHs were installed. Figure 1 illustrates the distribution of observation sites in this area. For more details of AMPEX, please visit the following website: http://home.hiroshima-u.ac.jp/~ampex/hm/index-e.htm.

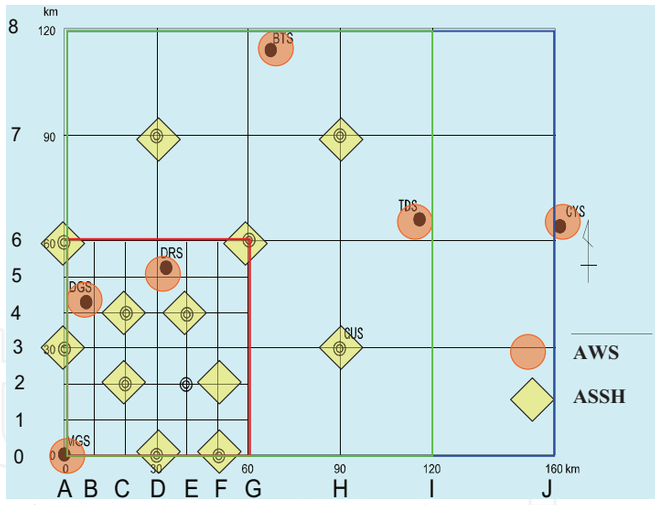

Fig. 1. Distribution of ASSH and AWS in AMPEX study area

The ASSHs provide soil moisture and temperature profile measured at two depths, 3 cm and 10 cm below the surface. The AWSs provide soil moisture and temperature profiles measured at four depths: 3 cm, 10 cm, 40 cm and 100 cm below the surface. The soil moisture measurements used TDRs, and the soil temperature was measured by platinum resistance thermometers.

Through matching the AMSR-E footprints to in situ stations, we generated a match-up data set consisting of brightness temperature data observed by AMSR-E and in situ data

measured by SMTMS and AWS. The coverage of this data set is 2.5 by 2.5 degrees, with a resolution 0.05 degrees for all frequencies. The in situ data consists of soil moisture and soil temperature data. It is in the form of an image type and a text type. The text files record AMSR-E brightness temperature and in situ data at each ground station. The in situ data include observations made within 12 hours of the AMSR-E observation. In this research, the mach-up in situ data at each AMSR-E satellite over passing is calculated by interpolating the in situ data on the hour.

Based on the AMSR 2002 field experiment results, the soil bulk density in this region is 1.258 $g \bullet cm^{-3}$. The soil texture is obtained from the Net Primary Productivity (NPP) Database (Chuluun & Ojima, 1996): a sand fraction of 0.6, a silt fraction of 0.2 and a clay fraction of 0.2. There is sparse vegetation in study area. The vegetation water content was measured in June and August, 2003. Based on this in situ observation, we found that the maximum vegetation water content in our study area was 0.11 $kg \bullet m^{-2}$. It is a small value reflecting the sparse vegetation coverage.

4.2 Best-fitting parameters for AMSR-E

With the AMSR-E match-up data, the land surface parameters can be obtained easily by using the best-fitting methods. AMSR-E TB data obtained from low frequency channels (6.925, 10.65 and 18.7 GHz) were used to optimize model parameters. Since the wavelength of those channels is generally much larger than the diameter of atmospheric particles, the atmospheric effect is negligible for the data measured with those channels.

As reported in the literature, it is reasonable to assume that there is little or no volume scattering for soil moisture levels over 10% (Ulaby et al., 1986). So, we first used the data observed on wet days to estimate the roughness parameters, *rms* height and correlation length, in a best-fitting way. The particle size parameter could then be obtained by running a coupled DMRT-AIEM model to best fit the data observed on dry days.

In order to run DMRT, we used uniform soil moisture and temperature vertical profiles with the value observed at 3 cm depth. The bottom of the soil medium was set to be 1.0m (layer thickness is 1cm) and the brightness temperature at the bottom was assumed to be the soil physical temperature at that level, that is, the emissivity was equal to one. The downward radiation from each soil layer, reflected at the bottom boundary, was not considered in this study. The interactions at the boundaries between neighboring soil layers were also neglected because of the vertically uniform soil moisture and temperature profiles.

First, we used the AIEM model to best fit several wet day observations by changing *rms* height (s) and correlation length (l). Second, employing this set of s and l, we could obtain the surface emissivity for all observations. Third, with some dry day observations, we could best fit the particle size parameter using the DMRT-AIEM model. Finally, we calculated brightness temperature from April 10th 2003 to April 30th 2004 with best-fitting parameters.

Here, we use the A3 station as an example, to introduce the whole procedure and the result. Information about the data we used to calibrate the model is listed in following table.

cases	Number of days	Mv range (%)	T(3cm) range	Period
Wet	32	10~20	275.26~291.25	May. 12th ~ Aug. 20th ,03
Dry	40	1~7	273.1~293.8	Apr.14th~Jul.13th,03
ALL	254	1~20	270~293.8	Apr. 12th,03 ~Apr, 30th, 04

Table 1. Data used for parameter optimization

The calibrated parameter values of AIEM with consideration of shadowing effects are: s = *0.46 cm*; l = *1.03 cm*. Then, with this set of s and l, using data for 40 dry days, we best fit the particle size parameter as in table 2:

F(GHz)	6.925	10.65	18.7	23.8	36.5
Wave Length λ (cm)	1.997	1.298	0.739	0.581	0.379
R(cm)	0.45	0.307	0.165	0.126	0.084
R/λ	0.104	0.109	0.103	0.100	0.102

Table 2. Best-fitting particle size parameters in Mongolia

As in Table 2, the best-fit particle sizes change at different frequencies: longer wavelengths are matched with larger particle sizes. However, the ratio between the best-fit radius and the wavelength in the sand is nearly constant. Therefore, we call the best-fit radius the effective radius. The effective radii are generally larger than the physical values, consistent with similar results reported by Kendra and Sarabandi (1999).

4.3 AMSR-E Look up table generation

Based on the best-fitted parameter sets, we build a lookup table composed of the soil physical temperature, soil moisture content, brightness temperature at 10.65GHz vertical polarization and an index *dTB* calculated as follows:

$$dTB = TB(18.7, H) - TB(10.65, H) \tag{9}$$

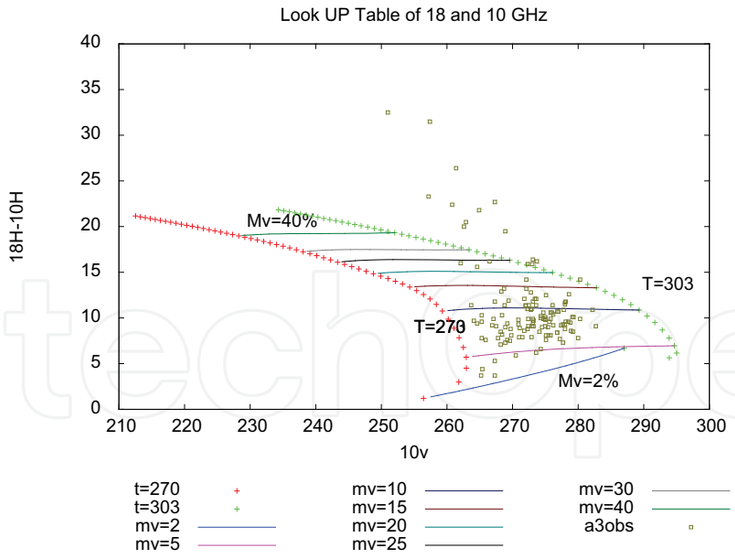

Fig. 2. Lookup table for the AMSR-E soil moisture retrieval algorithm

The lookup table of our AMSR-E algorithm is shown in **Figure 2**. It covers a region in which soil moisture content varies from 2% to 40%, and soil physical temperature varies from 270K to 303K. Compared with in situ observation values, this range is large enough to include all of the actual soil moisture and temperature states in Mongolia.

Since the one-to-one relationship in our lookup table is very clear, it becomes simple to reverse the lookup table, so that the soil moisture can easily be estimated from the AMSR-E data set.

4.4 Retrieval soil moisture from AMSR-E

In this study, we retrieved soil moisture data for the period from July to August, 2003. The estimation is shown in **Figure 3** for (a) time variation and (b) accuracy comparison.

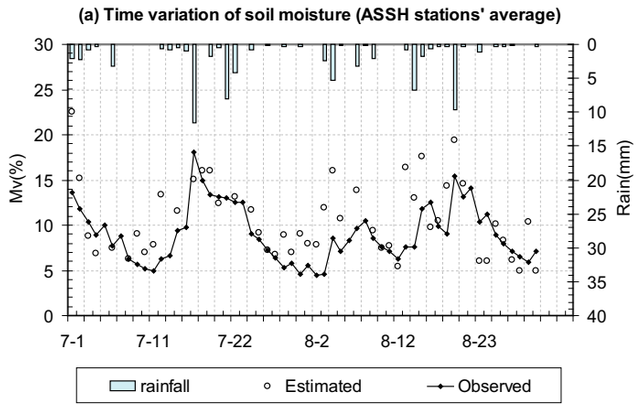

Fig. 3(a). Time series of retrieved soil moisture, observed soil moisture and precipitation.

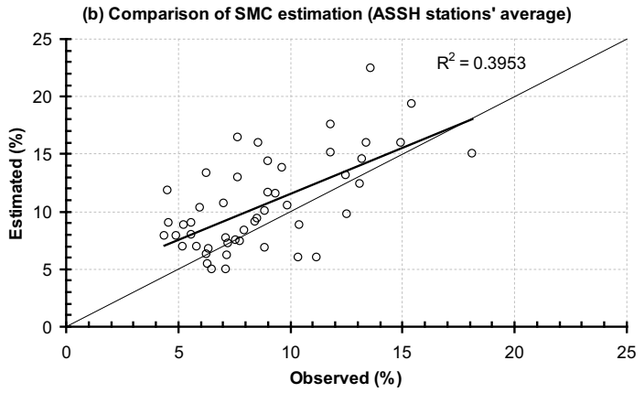

Fig. 3(b). Comparison of retrieval results with in situ observation

It is clear from **figure 3** that the algorithm gives a reliable soil moisture content estimate in both tendency and amplitude. The value of R-square is 0.3953, and the Standard Error of the Estimate (SEE) is 3.8%. From **figure 3(a)**, we find some overestimation around Aug. 4, 14 and 20, when moderate rainfall (5~10 mm) occurred. Such errors can be attributed partly to the difference between the TDR sensor depth and the penetration depth of the X band and Ku band. Moderate rainfall makes the soil surface much wetter than the soil 3cm below the surface where the TDR sensors were located. Such vertical heterogeneity of soil moisture in the first 3cm of soil was not considered in our algorithm. On the other hand, the wet surface situation decreases the penetration depth dramatically. The combination of these reasons makes our algorithm estimate higher soil moisture content than the in situ observations for moderate rainfall periods.

One advantage of our proposed algorithm is that it estimates soil physical temperature and soil moisture simultaneously. This is important for studies involving energy and water budget, such as studies of land surface processes and of weather forecasting.
The average retrieved physical temperature for ASSH stations is shown in **figure 4(a)** and **figure 4(b)**. As in soil moisture comparisons, the algorithm effectively retrieved physical temperature on average for 10 stations. The value of R-square is 0.5458, and the value of SEE is 4.4K. As with our soil moisture analysis, the overestimation of daily temperature variation can also be explained partly as the results of different observation depths.

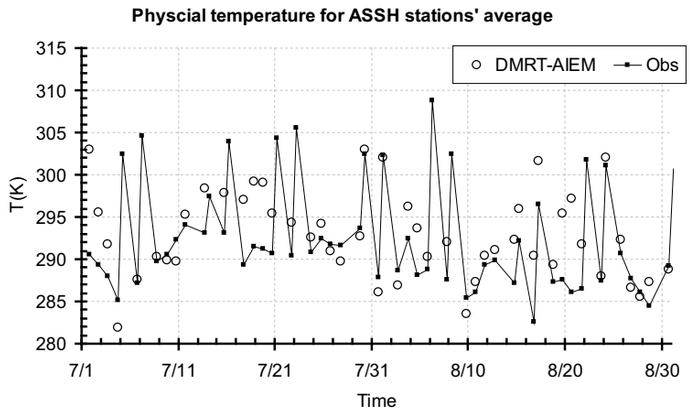

Fig. 4(a). Time series of retrieved and in situ observations of soil physical temperature.

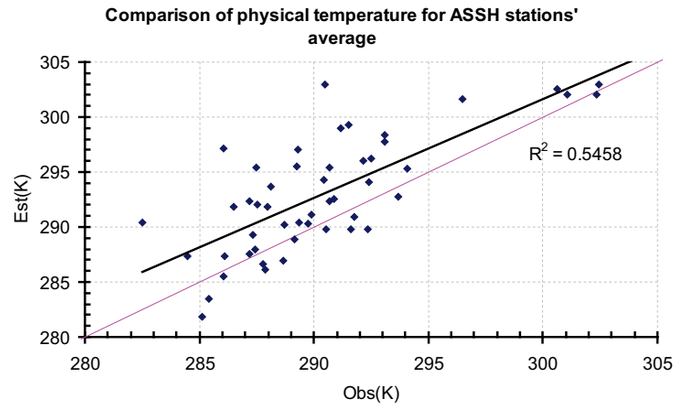

Fig. 4(b) Comparison of algorithm-estimated soil physical temperature with in situ observation

5. Application to SSM/I

Since the parameters used in our RTM have clear physical meaning, they are independent on the configuration of radiometers. The parameters used in AMSR-E soil moisture retrieval therefore can be directly used to the SSM/I data set, in the same region. In this test, we first checked the accuracy of TB simulation of our DMRT-AIEM model. And then a look up table for SSM/I data was generated and soil moisture was retrieved.

5.1 SSM/I TB Validation

Using the parameters optimized by AMSR-E math-up data set, with the in-situ observed soil moisture and temperature as input, we run the DMRT-AIEM model to generate TB at 19.35 and 37.0 GHz, two frequencies operated by SSM/I. The SSM/I TB validation results were shown in figure 5, for the A3 station, during the period from Jul. 1st to Jul. 30th, 2003.

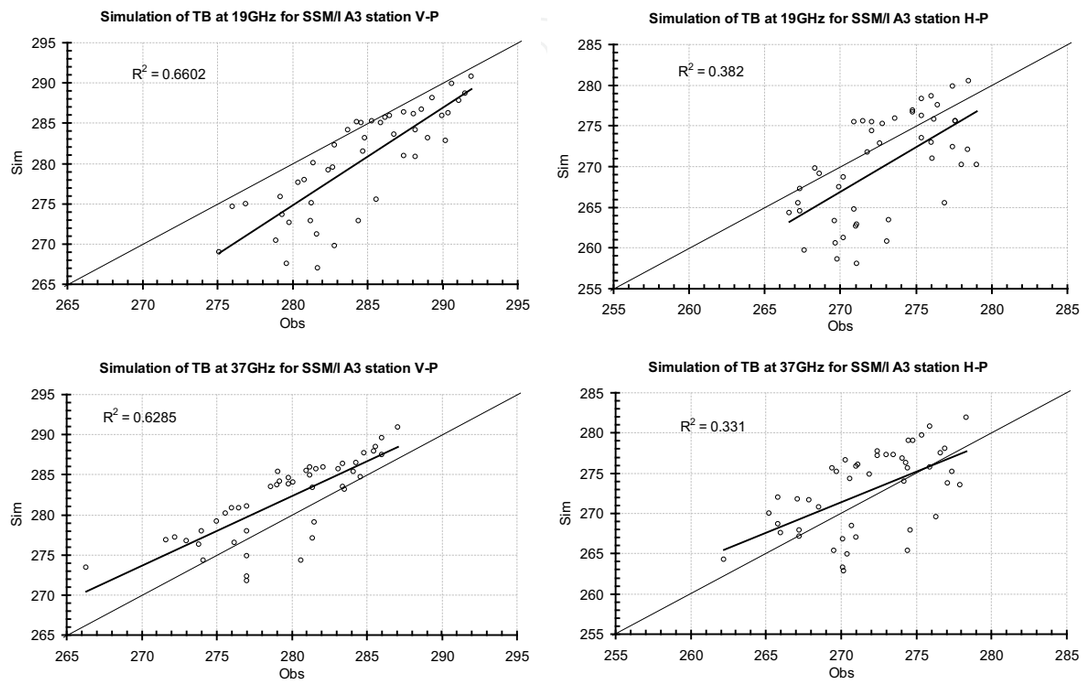

Fig. 5. Comparison of simulated brightness temperature with the one observed by SSM/I

From figure 5, it is clear that, for the vertical polarization, the TB simulated by DMRT-AIEM is in a good correlation with the SSM/I observation, with slight underestimation for 19 GHz and overestimation for 37 GHz. For the horizontal polarization, the performance of our RTM is not so good. Statistically, the Average Absolute Error (AAE, see equation (10)) and the square of correlation coefficient between observed brightness temperature and simulated one are listed in table 3.

Channel	19V	19H	37V	37H
AAE (K)	4.34	4.41	3.45	3.85
R^2	0.66	0.38	0.63	0.33

Table 3. AAE and correlation coefficient of DMRT-AIEM model for SSM/I data

$$AAE = \{\sum_{i=1}^{n}[ABS(TBS_{i,V} - TBO_{i,V}) + ABS(TBS_{i,H} - TBO_{i,H})]\}/(n*2) \quad (10)$$

where, *TBS* is simulated brightness temperature, *TBO* is observed brightness temperature by spaceborne sensor; *n* is number of samples.

5.2 Look up table of SSM/I

Through the TB validation, it was confirmed that our DMRT-AIEM model was able to produce reasonable TB at vertical polarization channels of SSM/I. But there was some gaps between the simulated TB with the one observed by SSM/I, especially for horizontal polarization channels. Moreover, as we know, the atmosphere effects should be considered for 37 GHz. All of these make it difficult to build a look up table with the same way used for AMSR-E. Authors proposed a simple solution by nudging the SSM/I TB data to fit the simulation and by using PI and ISW indexes to generate a look up table. Detail of the TB adjustments and look up table generation can be found from (Ohta et al., 2007). Figure 6 shows the look up table for SSM/I, in which the PI calculated from 19 GHz and the ISW calculated from the horizontal polarization of 37 and 19 GHz were used. The black points represent the PI and ISW values calculated from corresponding TB data observed by SSM/I.

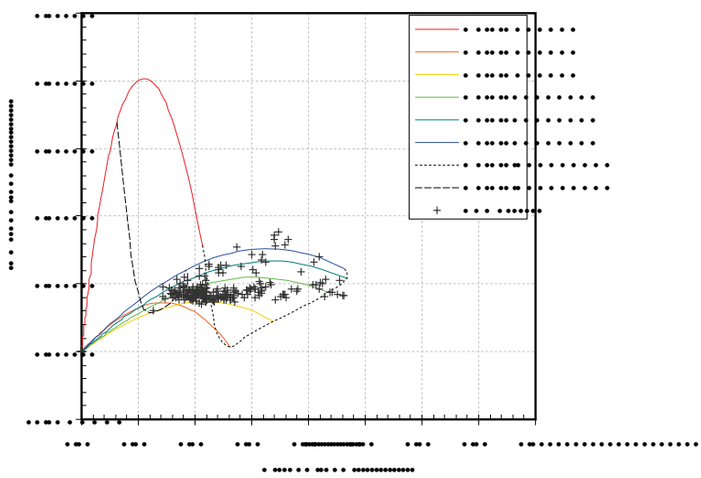

Fig. 6. Diagram of the Look Up Table for SSM/I soil moisture algorithm

5.3 Soil moisture retrieval from SSM/I

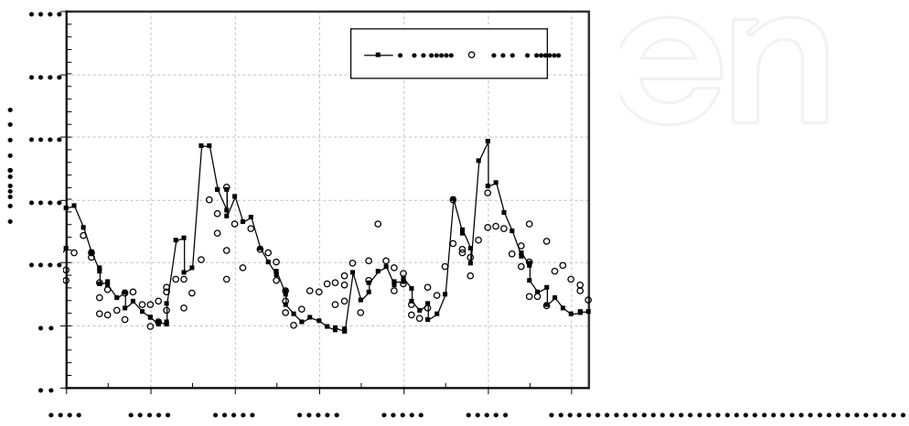

Fig. 7. Comparison of soil moisture retrieved from SSM/I with in-situ observation

By using the PI-ISW look up table, soil moisture was estimated from SSM/I TB data. The results are shown in figure 7, for the period from July to August, 2003. The line represents the in-situ soil moisture observation; the open cycles are SSM/I soil moisture estimate. From this figure, it is clear that the performance of SSM/I soil moisture retrieval algorithm is very good. So, it is feasible to get reasonable soil moisture estimation form SSM/I with the helps from AMSR-E. But we must keep it in mind that the TB adjustment was applied to the SSM/I data. Such good performance of SSM/I algorithm is therefore just for the special cases where the in-situ observation are available and the appropriate TB adjustment are possible.

6. Conclusions

Spatial distributed soil moisture information is an essential parameter for hydrological, meteorological and ecological studies. This paper presents the structure and contents of a soil moisture retrieval algorithm for the spaceborne passive microwave remote sensing. This algorithm was validated by using the AMSR-E match-up data set at CEOP Mongolia reference site. Comparing to the in-situ observation, reliable surface soil moisture was retrieved by the algorithm.

The transferability of our algorithm was also tested by using SSM/I TB data. At first, it was demonstrated that the forward RTM of our algorithm was capable to represent the SSM/I TB data only after the parameters were calibrated by AMSR-E data set. And then, with some adjustments to the SSM/I TB data, reasonable surface soil moisture was also retrieved from SSM/I data by our algorithm.

The results presented in this paper clearly show that we had built a bridge between the parameters retrieved from AMSR-E and those for SSM/I. With some further consideration about the difference between AMSR-E and SSM/I, e.g. the footprint size and the observation patterns, it is believed that our algorithm could provide a possibility to use the long historical global data observed by SSM/I. Moreover, it is possible to extend our algorithm to other available radiometers. And then, we can merge multi-sensor or/and multi-satellite observations to generate a long term global historical soil moisture product. Such a long term historic data set should be much useful for large scale hydrological and climatologic studies.

As mentioned in section 1, the retrieval of surface soil moisture is physically limited by the current satellite instruments which are operating at high frequencies. The low frequency, i.e. L-band, passive microwave soil moisture observation will firstly be available through the launch of Soil Moisture Ocean Salinity (SMOS) mission of ESA (Kerr, et al., 2001). NASA will provide a combined L-band radiometer and L-band radar observation through the Soil Moisture Active and Passive (SMAP) mission (Entekhabi, et al., 2008). Since the configuration of our algorithm was not specified to any sensors, it is also possible to apply our algorithm to the incoming L-band radiometers. We hope this algorithm will be helpful for these future soil moisture missions and for connecting current available C-band and X-band observations to the L-band observations.

7. Acknowledgements

This study was carried out as part of the Coordinated Enhanced Observing Period (CEOP) and Verification Experiment for AMSR/AMSR-E funded by the Japanese Science and

Technology Corporation for Promoting Science and Technology Japan and by the Japan Aerospace Exploration Agency (JAXA). The authors express their great gratitude to them.

8. References

Beljaars, A.C.M.; Viterbo P.; Miller M.j. & Betts A.J. (1996). The anomalous rainfall over the United States during July 1993: sensitivity to land surface parameterization and soil moisture anomalies. *Monthly Weather Review*, 124, 362-383.

Burke, W.J.; Schmugge, T.J. & Paris, J.F. (1979). Comparison of 2.8 and 21 cm microwave radiometer observations over soils with emission model calculation. *Journal of Geophysics Research*, 84, 287-294.

Chen, K.S.; Wu, T.D.; Tsang, L.; Li, Q.; Shi, J.C. & Fung, A.K. (2003). Emission of rough surfaces calculated by the integral equation method with comparison to three-dimensional moment method simulations. *IEEE Transactions on Geoscience and Remote Sensing*, 41, 90-101.

Choudhury, B. J.; Schmugge, T.J.; Chang, ATC & Newton N.R. (1979). Effect of surface roughness on the microwave emission from soils. *Journal of Geophysical Research*, *84*, 5699-5706.

Chuluun, Togtohyn & Ojima, D.S. (1996). Simulation studies of grazing in the Mongolian steppe, *Proceedings of the fifth International Rangeland Congress*, Society of Range Management, Denver, CO, USA.

Dobson, M.C.; Ulaby, F.T.; Hallikainen, M.T. & Elrayes, M.A. (1985). Microwave dielectric behavior of wet soil .2. dielectric mixing models. *IEEE Transactions on Geoscience and Remote Sensing* 23, 35-46.

Delworth, T. & Manabe, S. (1988). The influence of potential evaporation on the variability of simulated soil wetness and climate. *Journal of Climate*, 13, 2900−2922.

Entekhabi, D.; Rodrigues-Iturbe I. & Castelli F. (1996). Mutual interaction of soil moisture state and atmospheric processes. *Journal of Hydrology*, 184, 3-17.

Entekhabi, D.; Njoku, E.; Oneill, P. E.; Spencer, M.; Jackson, T.; Entin, J.; Im, E. & Kellogg, K. (2008). The Siol Active Passive Mission (SMAP). *Proceedings of the IEEE 2008 International Geoscience and Remote Sensing Symposium* (IGARSS'08), 3, 1–4, July, 2008, Boston, Doi: 10.1109/IGARSS.2008.4779267.

Fung, A.K.; Li, Z.Q. & Chen, K.S. (1992). Backscattering from a randomly rough dielectric surface. *IEEE Transactions on Geoscience and Remote Sensing*, 30, 356-369.

Gloersen, P. & Barath F. T. (1977). A Scanning Multichannel Microwave Radiometer for Nimbus-G and SeaSat-A. *IEEE Journal of Oceanic Engineering*, 2:172-178.

Henyey, L. C. & Greenstein, J. L. (1941). Diffuse radiation in the galaxy, *The Astrophysics Journal*, 93, 70–83.

Hipp J.E. (1974). Soil electromagnetic parameters as functions of frequency, soil density, and soil moisture, *Proceedings of the IEEE*, 62:98–103

Hollinger, J.P.; Peirce, J.L. & Poe, G.A. (1990). SSM/I Instrument Evaluation. *IEEE Transactions on Geoscience and Remote Sensing*, 28(5), 781-790.

Jackson, T. J. & Oneill, P. E. (1990). Attenuation of Soil Microwave Emission by Corn and Soybeans at 1.4 Ghz and 5 Ghz. *IEEE Transactions on Geoscience and Remote Sensing,* **28**(5), 978-980.

Jackson, T.J. & Schmugge, T.J. (1991). Vegetation effects on the microwave emission of soils. *Remote Sensing of Environment*, 36, 203-212.

Jackson, T.J. (1993). Measuring surface soil moisture using passive microwave remote sensing. *Hydrology Processes*, 7, 139-152.

Kawanishi,T.; Sezai, T.;Ito Y.; Imaoka, K.; Takeshima, T.; Ishido, Y.; Shibata, A.; Miura, M.; Inahata, H. & Spencer Roy W. (2003). The advanced microwave scanning radiometer for the earth observing system (AMSR-E), NASDA's contribution to the EOS for global energy and water cycle studies. *IEEE Transactions on Geoscience and Remote Sensing*, 41, 184-194.

Kendra, J. R. & Sarabandi, K. (1999). A hybrid experimental theoretical scattering model for dense random media. *IEEE Transactions on Geoscience and Remote Sensing*, 37, 21-35.

Kerr, Y. H.; Waldteufel, P.; Wigneron, J. P.; Martinuzzi, J. M.; Font, J. & Berger, M. (2001). Soil moisture retrieval from space: The Soil Moisture and Ocean Salinity (SMOS) mission. *IEEE Transactions on Geoscience and Remote Sensing*, **39,** 1729-1735

Koike, T.; Tsukamoto, T.; Kumakura, T. & Lu, M. (1996). Spatial and seasonal distribution of surface wetness derived from satellite data, *Proceedings of International workshop on macro-scale hydrological modeling*, 87-96.

Koike, T. (2004). The Coordinated Enhanced Observing Period – an initial step for integrated global water cycle observation, *WMO Bulletin*, 53(2), 1-8.

Liu, G. (1998). A fast and accurate model for microwave radiance calculations, Journal of Meteorology Society of Japan, 76(2), 335–343.

Lu, H.; Koike, T.; Hirose, N.; Morita, M.; Fujii, H.; Kuria, D. N.; Graf, T. and Tsutsui, H. (2006). A basic study on soil moisture algorithm using ground-based observations under dry condition. *Annual Journal of Hydraulic Engineering, Japan Society of Civil Engineer*, 50, 7-12.

Lu, H.; Koike, T.; Fujii, H.; Ohta, T. & Tamagawa, K. (2009). Development of a Physically-based Soil Moisture Retrival Algorithm for Spaceborne Passive Microwave Radiometers and its Application to AMSR-E, *Journal of The Remote Sensing Society of Japan*, 29(1), 253-261.

Mironov, V.L.; Dobson, C.; Kaupp, V.H.; Komarov, V.A. & Kleshchenko, V.N. (2004). Generalized refractive mixing dielectric model for moist soils. *IEEE Transactions on Geosciences and Remote Sensing*, 42:773–785. doi:10.1109/TGRS.2003.823288

Mo, T. & Schmugge, T. J. (1987). A Parameterization of the Effect of Surface-Roughness on Microwave Emission. *IEEE Transactions on Geoscience and Remote Sensing*, **25**(4), 481-486

Njoku, E.G. & Kong, J.A. (1977). Theory for passive microwave remote sensing of near-surface soil moisture. *Journal of Geophysical Research*, 82, 3108-3118.

Njoku, E.G. & Entekhabi, D. (1996). Passive microwave remote sensing of soil moisture. *Journal of Hydrology*, 184, 101-129.

Njoku, E.G.; Jackson, T.J.; Lakshmi, V.; Chan, T.K. & Nghiem, S.V. (2003). Soil moisture retrieval from AMSR-E. *IEEE Transactions on Geoscience and Remote Sensing*, 41, 215-229.

Oh, Y. & Kay, Y. C. (1998). Condition for precise measurement of soil surface roughness. *IEEE Transactions on Geoscience and Remote Sensing*, **36**(2), 691-695.

Ohta, T; Koike, T.; Lu, H.; Kuria, D.N.; Tsutsui, H.; Graf, T.; Kaihotsu, I; Davaa, G. & Matsuura, N. (2007). Development of a special sensor microwave imager (SSM/I)

algorithm for long term monitoring of soil moisture, *Annual Journal of Hydraulic Engineering, Japan Society of Civil Engineer*, 51, 205-210.

Owe, M.; De Jeu, R.A.M. & Holmes, T.R.H. (2008). Multi-sensor historical climatology of satellite-derived global land surface moisture. *Journal of Geophysics Research*, 113, doi:10.1029/2007JF000769.

Paloscia, S. & Pampaloni, P. (1988). Microwave polarization index for monitoring vegetation growth. *IEEE Transactions on Geoscience and Remote Sensing*, 26, 617-621.

Paloscia, S.; Macelloni, G.; Santi, E. & Koike, T. (2001). A multifrequency algorithm for the retrieval of soil moisture on a large scale using microwave data from SMMR and SSM/I satellites, *IEEE Transactions on Geoscience and Remote Sensing*, 39, 1655~1661.

Paloscia, S.; Macelloni, G. & Santi E. (2006). Soil moisture estimates from AMSR-E brightness temperatures by using a dual-frequency algorithm, *IEEE Transactions on Geoscience and Remote Sensing*, 41(11), 3135-3144.

Prigent, C.; Aires, F.; Rossow, W. B. & Robock, A. (2005). Sensitivity of satellite microwave and infrared observations to soil moisture at a global scale: Relationship of satellite observations to in situ soil moisture measurements. *Journal of Geophysical Research*, 110, D07110. doi:10.1029/2004JD005087

Ray, P. S. (1972). Broadband Complex Refractive Indices of Ice and Water. *Applied Optics*, 11 (8), 1836-1844.

Said, S., Kothyari, U.C. & Arora, M.K. (2008). ANN-based soil moisture retrieval over bare and vegetated areas using ERS-2 SAR data. *Journal of Hydrologic Engineering*, 13, 461-475.

Schar, C.; Luthi, D.; Beyerle, U. & Heise, E. (1999). The soil-precipitation feedback: A process study with a regional climate model. *Journal of Climate*, 12, 722−741.

Schmugge, T.J. & Choudhury B.J. (1981). A comparison of radiative transfer models for predicting the microwave emission from soils. *Radio Science*, 16, 927-938.

Schmugge, T.J.; Wang, J.R. & Asrar G. (1988). Results from the Push Broom Microwave Radiometer flights over the Konza Prairie in 1985. *IEEE Transactions on Geoscience and Remote Sensing*, 26(5), 590–597.

Schmugge, T. J. & Jackson, T. J. (1992). A Dielectric Model of the Vegetation Effects on the Microwave Emission from Soils. *IEEE Transactions on Geoscience and Remote Sensing*, **30**(4), 757-760.

Seneviratne, S. I.; Luthi, D.; Litschi, M. & Schar, C. (2006). Land–atmosphere coupling and climate change in Europe. *Natur*e, 443(7108), 205−209.

Shi, J. C.; Jiang, L.M.; Zhang, L.X.; Chen, K.S.; Wigneron, J.P. & Chanzy, A. (2005). A parameterized multifrequency-polarization surface emission model, *IEEE Transactions on Geoscience and Remote Sensing,* 43, 2831-2841.

Shibata, A.; Imaoka, K. & Koike, T. (2003). AMSR/AMSR-E level 2 and 3 algorithm developments and data validation plans of NASDA. *IEEE Transactions on Geoscience and Remote Sensing,* 41, 195-203

Singh, D.; Sing, K. P.; Herlin, I. & Sharma, S.K. (2003). Ground-based scatterometer measurements of periodic surface roughness and correlation length for remote sensing. *Advances in Space Research*, **32**(11), 2281-2286.

Singh, D. & Kathpalia, A. (2007). An efficient modeling with GA approach to retrieve soil texture, moisture and roughness from ERS-2 SAR data. *Progress in Electromagnetics Research-Pier*, 77, 121-136.

Tsang, L. & Kong, J. A (1977). Theory for thermal microwave emission from a bounded medium containing spherical scatterers, *Journal of Applied Physics*, 48, 3593-3599.

Tsang, L. & Kong, J. A (2001). *Scattering of Electomagnetic Waves: Advanced Topics*, Wiley, New York.

Ulaby, F.T.; Razani, M. & Dobson, M.C. (1983). Effects of vegetation cover on the microwave radiometric sensitivity to soil moisture. *IEEE Transactions on Geoscience and Remote Sensing*, 21, 51-61.

Ulaby, F.T. ; Moore, R.K & Fung A.K. (1986). *Microwave Remote Sensing: Active and Passive*, Artech House, Norwood, MA.

Verstraeten, W.W.; Veroustraete, F.; van der Sande, C.J.; Grootaers, I. & Feyen, J. (2006). Soil moisture retrieval using thermal inertia, determined with visible and thermal spaceborne data, validated for European forests. *Remote Sensing of Environment*, 101, 299-314.

Wagner, W.; Scipal, K.; Pathe, C.; Gerten, D.; Lucht, W. & Rudolf, B. (2003). Evaluation of the agreement between the first global remotely sensed soil moisture data with model and precipitation data. *Journal of Geophysical Research*, 108(D19), 4611- , doi:10.1029/2003JD003663

Wang, J.R. & Schmugge, T.J. (1980). An empirical model for the complex dielectric permittivity of soils as a function of water content. *IEEE Transactions on Geoscience and Remote Sensing*, 18, 288-295.

Wang, J. R. & Choudhury, B. J. (1981). Remote-Sensing of Soil-Moisture Content over Bare Field at 1.4 Ghz Frequency. *Journal of Geophysical Research-Oceans and Atmospheres*, **86** (Nc6), 5277-5282.

Wegmuller, U. & Matzler, C. (1999). Rough bare soil reflectivity model. *IEEE Transactions on Geoscience and Remote Sensing*, 37, 1391-1395.

Wen, B.; Tsang, L.; Winebrenner, D. P. and Ishimura, A. (1990). Dense media radiative transfer theory: comparison with experiment and application to microwave remote sensing and polarimetry, *IEEE Transactions on Geoscience and Remote Sensing*, 28, 46-59.

Wigneron, J. P.; Laguerre, L. & Kerr, Y. (2001). A simple parameterization of the L-band microwave emission from rough agricultural soils. *IEEE Transactions on Geoscience and Remote Sensing,* **39**(8), 1697-1707.

Yang, K.; Watanabe, T.; Koike, T.; Li, X.; Fujii, H.; Tamagawa, K.; Ma Y. & Ishikawa H. (2007). An auto-calibration system to assimilate AMSR-E data into a land surface model for estimating soil moisture and surface energy budget. *Journal of Meteorology Society of Japan*, 85A, 229-242.

Yang, K.; Koike, T.; Kaihotsu, I. & Qin, J. (2009). Validation of a Dual-pass Microwave Land Data Assimilation System for Estimating Surface Soil Moisture in Semi-arid Regions, *Journal of Hydrometeorology*, 10(3), 780-794.

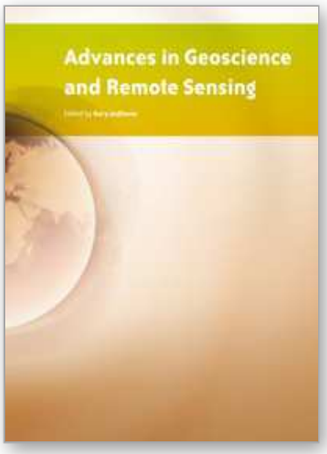

Advances in Geoscience and Remote Sensing

Edited by Gary Jedlovec

ISBN 978-953-307-005-6

Hard cover, 742 pages

Publisher InTech

Published online 01, October, 2009

Published in print edition October, 2009

Remote sensing is the acquisition of information of an object or phenomenon, by the use of either recording or real-time sensing device(s), that is not in physical or intimate contact with the object (such as by way of aircraft, spacecraft, satellite, buoy, or ship). In practice, remote sensing is the stand-off collection through the use of a variety of devices for gathering information on a given object or area. Human existence is dependent on our ability to understand, utilize, manage and maintain the environment we live in - Geoscience is the science that seeks to achieve these goals. This book is a collection of contributions from world-class scientists, engineers and educators engaged in the fields of geoscience and remote sensing.

INTECH
open science | open minds

InTech Europe
University Campus STeP Ri
Slavka Krautzeka 83/A
51000 Rijeka, Croatia
Phone: +385 (51) 770 447
Fax: +385 (51) 686 166
www.intechopen.com

InTech China
Unit 405, Office Block, Hotel Equatorial Shanghai
No.65, Yan An Road (West), Shanghai, 200040, China
中国上海市延安西路65号上海国际贵都大饭店办公楼405单元
Phone: +86-21-62489820
Fax: +86-21-62489821

IntechOpen